Magnetism and Heterogeneous Catalysis: in depth on the quantum spin exchange interactions in Pt_3M (M= V, Cr, Mn, Fe, Co, Ni and Y)(111) alloys

Chiara Biz[ǂ], Mauro Fianchini[†], Victor Polo[‡], Jose Gracia[§,*]

[ǂ]Universitat Jaume I, Av. Vicente Sos Baynat s/n, E-12071 Castellón de la Plana, Spain

[†]Institute of Chemical Research of Catalonia (ICIQ), The Barcelona Institute of Technology, Avgda Països Catalans 16, 43007 Tarragona, Spain

[‡]Departamento de Química Física and Instituto de Biocomputación y Física de Sistemas Complejos (BIFI), Universidad de Zaragoza, Zaragoza, Spain

[§]MagnetoCat SL, General Polavieja 9 3I, 03012 Alicante, Spain

KEYWORDS. Heterogeneous catalysis, fuel cells, oxygen reduction reaction, quantum spin exchange interactions, Density Functional Theory, segregation

ABSTRACT. Bimetallic Pt-based alloys have drawn considerable attention in the last decades as catalysts in Proton Exchange Membrane Fuel Cells (PEMFCs), since they closely fulfill the two major requirements of high performance and good stability under operating conditions. Pt_3Fe, Pt_3Co and Pt_3Ni stand out as major candidates, given their good activity toward the challenging Oxygen Reduction Reaction (ORR). The common feature across catalysts based on *3d*-transition metals and their alloys is magnetism. Ferromagnetic spin-electron interactions, quantum spin exchange interactions (QSEI), are one of the most important energetic contributions in allowing milder chemisorption of reactants onto magnetic catalysts, in addition to spin-selective electron transport. The understanding of the role played by QSEI in the properties of magnetic *3d*-metals-based alloys is important to design and develop novel and effective electrocatalysts based on abundant and cheap metals. We present a detailed theoretical study (via Density Functional Theory) on the most experimentally explored bimetallic alloys Pt_3M (M = V, Cr, Mn, Fe, Co, Ni and Y)(111). The investigation starts with a thorough structural study on the composition of the layers, followed by a comprehensive physico-chemical description of their resistance towards segregation and their chemisorption capabilities towards hydrogen and oxygen atoms. Our study demonstrates that $Pt_3Fe(111)$, $Pt_3Co(111)$ and $Pt_3Ni(111)$ possess the same preferential multilayered structural organization, known for exhibiting specific magnetic properties. The specific role of QSEI in their catalytic behavior is justified via comparison between spin polarized and non-spin polarized calculations.

INTRODUCTION

Pt-based materials exhibit promising results as catalysts in PEMFCs,[1-3] smoothing the oxygen reduction reaction (ORR); that is the bottleneck hampering the development of these electrochemical devices.[1, 4] The most widely investigated compositions are $Pt_3M(111)$ alloys, where M is V, Cr, Mn, Fe, Co, Ni and Y metals.[1-2, 4] $Pt_3Fe(111)$, $Pt_3Co(111)$ and Pt_3Ni (111) are considered as the best Pt-based catalysts due to their optimal ORR activity and relatively good stability.[1,5-7] $Pt_3V(111)$ and $Pt_3Cr(111)$ are often claimed as potential catalysts, for their good robustness and durability under the operating catalytic conditions of the electrolytic cell.[2,8-9] $Pt_3Mn(111)$ remains the less investigated Pt-based catalyst, despite its various and interesting magnetic properties.[10] Few groups also mention the non-magnetic $Pt_3Y(111)$ alloy as potential candidate.[11-12]

The presence of heterometallic sublayers in a solid catalyst is well known to improve the catalytic properties of the surface composed by noble metals.[3,13-14] Such enhancement in activity is generally explained via as ligand,[15] strain[16] and ensemble effects[17] in heterogeneous catalysis. These chemical effects depend upon the type, the stoichiometry and the distribution of the heterometallic centers within the catalyst structure and influence electronic properties of the catalyst by tuning the surface chemisorption capabilities.[3,13-14] In the case of *3d*-metal alloys, however, these effects alone do not entirely explain the catalytic behavior towards ORR: they cannot explain, for instance, the enhanced catalytic behavior of $Pt_3Co(111)$ versus Pt(111).[18-20] The missing tale to the puzzle when dealing with *3d*-transition metals, rare earth metals and their alloys, is represented by the spin-dependent potentials shaping ferromagnetic and antiferromagnetic situations.[21]

The roots of magnetism reside in the correlated movement of electron charges and spins. The magnetic properties of *3d*-transion metals derive from correlated movements within the outer *3d*-shells, while the magnetic properties of rare earth metals derive from the inner *4f*-shells.[22-23] The magnetism originated from *4f*-electrons mildly affects the intermetallic chemical bond[23] (for the shielding action of the outer $5s^2 5p^6$ shells)[22], but

the magnetism expressed by the outer *3d*-electrons plays a pivotal role in describing the chemical properties of light transition metals and their related alloys.[23] A cooperative behavior known as collective magnetism[24] is a characteristic of ferromagnetic (FM, parallel spin alignment) and antiferromagnetic materials (AFM, antiparallel alignment);[25] it can only be explained through indirect exchange interactions.[26] These interactions, previously named Quantum Spin Exchange Interactions (QSEI)[27-28] are a non-classical quantum phenomenon arising from the imposition of the antisymmetric wave function as solution of the Schrödinger equation under Pauli exclusion principle.[26,29] The exchange couplings between electrons with the same spin orientation reduce their Coulomb repulsion,[23,30] thus stabilizing the overall structure.[30] In strongly correlated materials[31] with open-shell orbital configurations, QSEI among parallel spins can lower the enthalpy of adsorption/desorption of chemical species onto the surface (e.g., $\Delta H_{cat} = \Delta H_{cat+adsorbate*} - (\Delta H_{cat} + \Delta H_{adsorbate(gas)})$).

For *3d*-metals Pt-based catalysts, QSEIs become a very relevant electronic factor in determining the energetics and kinetics of heterogeneous catalytic processes.[20,27,32-34] Computational studies demonstrate that dominant FM interactions play a crucial role in ORR[35,36] and experiments confirmed the enhanced catalytic activity of magnetic particles in oxygen electro-catalysis, due to spin-dependent delocalization of the charge carriers.[37,38] The QSEI stabilizing effect can be also macroscopically boosted by an external magnetic field when magnetic oxides are involved.[39,40] Experiments demonstrate that the application of an external magnetic field can induce an overall improvement in the PEMFCs catalytic performance, by accelerating the oxygen transport toward the catalytic layer of the electrodes[41] or activating the hydrogen molecules[42] or aligning proton conductive channels in the fuel cell membrane.[43] In summary, exogenous and endogenous magnetic potentials must be unavoidably considered to achieve a comprehensive description of chemical, physical and thus catalytic properties.

In this paper, we performed a thorough Density Functional Theory (DFT) study on multilayered compositions for experimentally relevant Pt_3M (M=V, Cr, Mn, Fe, Co, Ni and Y)(111) alloys. Multilayered compositions received also substantial attention in modern spintronics.[44] We carried out a comprehensive chemisorption screening of hydrogen and oxygen atoms as useful descriptor to identify optimal solid ORR catalysts.[45] We also completed a segregation study to assess the thermodynamic stability of the most promising $Pt_3M(111)$ nanostructures. Spin polarized (DFT+U method) and non-spin polarized calculations are ubiquitously carried out to define the role of magnetism and particularly QSEI on the chemisorption properties of the alloys.

RESULTS AND DISCUSSION

Structural and magnetic properties of Pt_3M (M=V, Cr, Mn, Fe, Co, Ni and Y) (111) alloys. Figure 1 shows the results of the speciation study for Pt_3M (M=V, Cr, Mn, Fe, Co, Ni and Y)(111) alloys by using a six layers model. The presence of a Pt-skin surface is the common feature among all the most stable nanostructures investigated in every group, in excellent agreement with experimental data on Pt-based alloys.[46] The remaining five sublayers (in our slab models) are diversely populated depending on the *d*-metal dopant.

The two most stable $Pt_3V(111)$ structures show preference for G-type AFM ordering (43 investigated structures, see SI pp. S5-S8). The energetic gap between the most stable AFM and FM orderings is a non-negligible ~0.18 eV. A very similar trend is also observed for the two most stable $Pt_3Cr(111)$ structures: the preferred magnetic ordering in this case is C-type AFM (42 investigated structures, see SI pp. S18-S21). The energetic gap between the most stable AFM and FM orderings is ~0.79 eV. Remarkably, $Pt_3V(111)$ and $Pt_3Cr(111)$ possess the same *3d*-metal distribution: 50 % in the 2nd and 5th layers and 25% in the 3rd and 4th layers, respectively. The four most stable $Pt_3Mn(111)$ structures suggest the presence of G- and C-type AFM orderings (41 investigated structures, see SI pp. S31-S34). The energy gap between the most stable AFM and FM configurations corresponds to ~0.84 eV for all the four $Pt_3Mn(111)$ nanostructures. 50% of the magnetic *3d*-metals in $Pt_3Mn(111)$ are placed in the 2nd, 4th and 5th layers, respectively (Figure 1).

To our knowledge, a straightforward experimental comparison for the structure of $Pt_3V(111)$, $Pt_3Cr(111)$ and $Pt_3Mn(111)$ alloys is not available at present time. On the contrary, $Pt_3Fe(111)$, $Pt_3Co(111)$ and $Pt_3Ni(111)$ are the most experimentally investigated compositions. The four most stable $Pt_3Fe(111)$ structures present a very tiny difference in energy between A-type AFM and FM, with a gap of ~0.05 eV (39 investigated structures, see SI pp. S47-S50). The full characterization of $Pt_3Co(111)$ structures has been reported in a previous work, showing that the energies of A-type AFM and FM orderings differ by < 0.1 eV.[20] The same trend seen for $Pt_3Fe(111)$ and $Pt_3Co(111)$ is also observed for $Pt_3Ni(111)$. Four nanostructures stand out as the most stable ones (34 investigated structures, see SI pp. S68-S71). As in case of $Pt_3Fe(111)$ and $Pt_3Co(111)$, A-type AFM orderings in $Pt_3Ni(111)$ show negligible energetic differences compared to FM orderings, with gap < 0.1 eV. It is worth to point out that the same magnetic atoms-per-layer distribution, e.g. 2nd and 5th layers both populated at 75% by *3d*-metal atoms (Figure 1), is observed for iron, cobalt and nickel. The most stable nanostructures found for $Pt_3Fe(111)$, $Pt_3Co(111)$ and $Pt_3Ni(111)$ match with experimental data evidencing a sub-skin layer (2nd) enriched in Fe, Co and Ni atoms.[5-6] Even more so, the computed structure of $Pt_3Co(111)$ is in good agreement with recent published results reporting inner-layers compositions.[18,19] The four most stable non-magnetic $Pt_3Y(111)$ structures (Figure 1) display very disorganized cells, where the clear separation of the different layers blurs substantially (42 investigated structures, see SI pp. S89-S92).

$Pt_3Fe(111)$, $Pt_3Co(111)$ and $Pt_3Ni(111)$: multilayered structure. Figure 1 shows that $Pt_3Fe(111)$, $Pt_3Co(111)$ and $Pt_3Ni(111)$ possess the same four global minima characterized by the same *3d*-transition metals layered distribution within the six layers model. The percentage of Fe, Co and Ni within the 2nd and the 5th layer is a constant 75%, but with a different spatial distribution within these two layers for all the three alloys. Figure 2 displays the multilayered nanostructures for each most stable slab of Pt_3Fe, Pt_3Co[20] and Pt_3Ni in detail, correlated with distances between the magnetic and the non-magnetic layers for the FM and A-type AFM orderings, respectively. Thus, hereby proposed multilayer structure for Pt_3Fe, Pt_3Co and Pt_3Ni is the result of various benchmark carried out for each $Pt_3M(111)$ alloys under study. The same multilayered structural organization has been "tested" for Pt_3V (see SI pp. S6, samples 15 and 16), Pt_3Cr (see SI pp. S19, samples 13 and 15), Pt_3Mn (see SI pp. S32, samples 10 and 11) and Pt_3Y (see SI pp. S91, samples 28-

30), but ordered multilayered *3d*-atomic distribution did not result to be the most stable (e.g. the latter alloys are more "single-phased").

Multilayered structures composed by a sequence of magnetic and non-magnetic layers have been extensively studied in the modern spintronics[44] for their applications in magneto-optical storage devices.[47] Magnetic multilayer systems based on Fe, Co and Ni separated by a noble metal spacer (e.g. Pt, Pd, Ag) possess the perpendicular magnetic anisotropy (PMA),[47-50] a preferential magnetization direction perpendicular to the material's plane, that is very appealing for technological applications.[47] Fe, Co and Ni exhibit perpendicular anisotropy for magnetic layers less thick than 10 Å.[49] Orientation (111) seems to be always the preferred orientation.[47] Pt/Co systems displays the strongest PMA,[48] while Pt/Fe and Pt/Ni systems present a marked dependence on the temperature.[49,51]

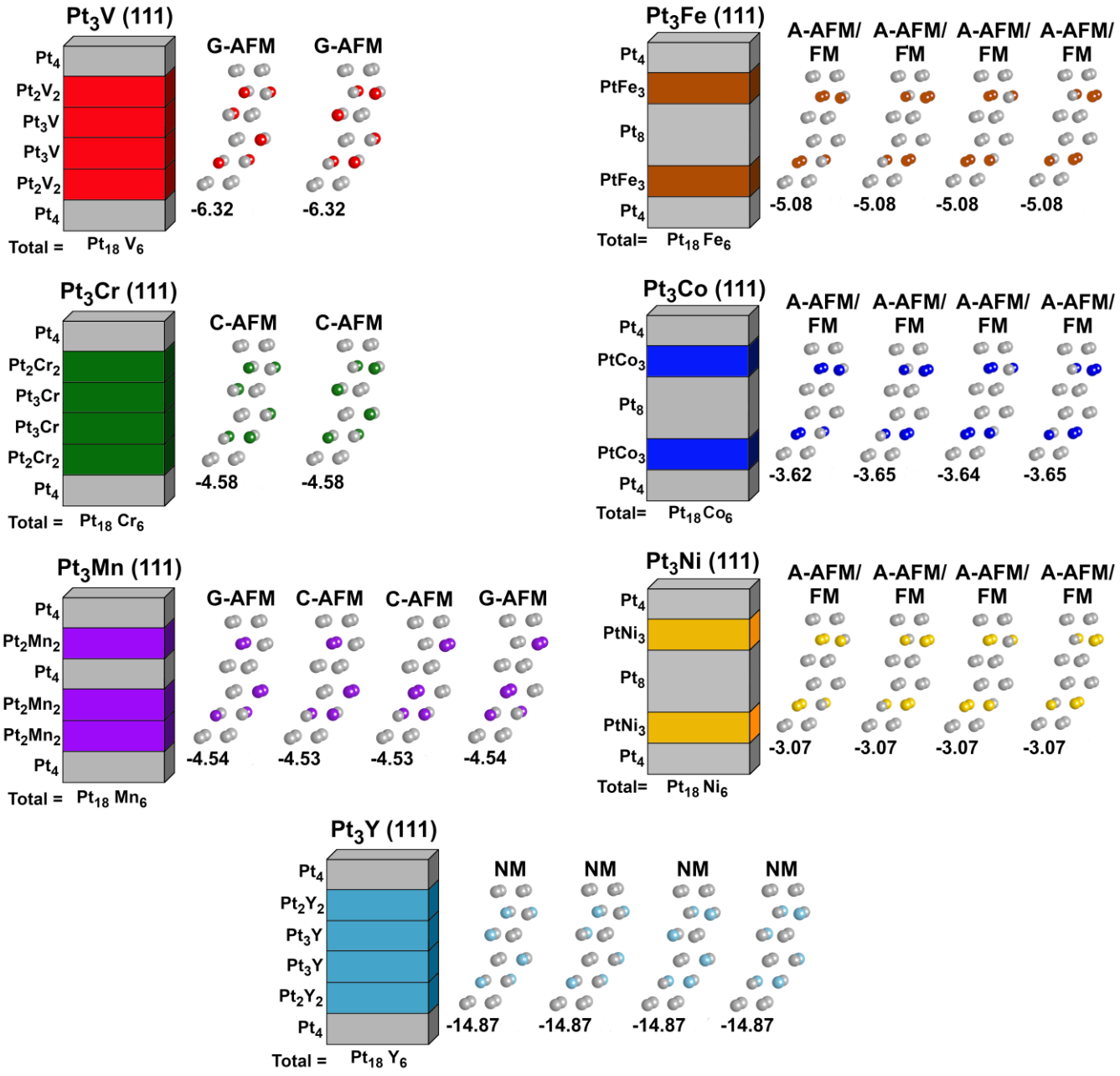

Figure 1. Sketch of structures, chemical compositions and magnetic orderings of the most stable nanostructures investigated for each bimetallic Pt_3M (M= V, Cr, Mn, Fe, Co, Ni and Y) (111) alloy. The numeric values beneath each slab represent its thermodynamic stability (ΔH) versus the most unstable slab found for each alloy, in eV. Density of States (DOS) for the most stable nanostructures are reported in SI p. S100.

Some authors explain the enhanced PMA in ultrathin Pt/Co systems with the formation of Pt-Co alloys at the interface.[48]

The same intermixing is claimed to play a minor role in Pt/Fe systems.[51] and even counterproductive in Pt/Ni systems (decrease of PMA).[52]

Multilayer systems also display interlayer exchange coupling.[53] In ultrathin Co and Fe multi-layered systems separated by Pt as non-magnetic spacer, the strength of the interlayer coupling experimentally depends on the thickness of the magnetic layers and usually decreases when the spacer thickness increases.[48,51] The interlayer exchange coupling originates at the interface in Pt/Co, where the magnetic Co atoms induce spin-polarization to the neighbor Pt centers and polarized interactions in adjacent Pt-Pt layers.[48] The polarization decreases in Pt/Fe systems[54] and appears to be even weaker in Pt/Ni,[49] lowering the interlayer coupling.

Chemisorption properties of Pt_3M (M=V, Cr, Mn, Fe, Co, Ni and Y) (111) alloys. The chemisorption energies of O_2*, O*, H* represent important parameters to rank catalytic effectiveness of potential solid catalysts.[45] We investigated the binding energies of adsorbed hydrogen ($\Delta H_{ads}^{H^*}$) and oxygen ($\Delta H_{ads}^{O^*}$) atoms onto the surface of $Pt_3M(111)$ alloys by identifying the structures providing the lowest energetically-demanding chemisorptions (non-magnetic Pt(111) is used as reference system). Published works suggest that the correlation between chemisorption and reactivity can be successfully constructed for oxygen reduction reaction, leading to the establishment of reactivity trends,[55] while such trends are still unclear for other reactions, like oxygen evolution reaction (e.g., particularly for simple oxides, where many more factors, like the creation of vacancies, the change of the phases, the changes valency states, the extrusion of oxygen atoms from bulk and surface, should be considered in a successful model. An interesting case is represented by Co_3O_4, that shows an anomalous behavior in OER,[55] but a top performance in ORR[56]). According to other published works, an optimal catalyst should display adsorbate-surface interaction strength in the "right" range.[45] For instance, this "right" range of O* chemisorption should correspond to values between 0.0 and 0.4 eV below the one exhibited by Pt(111) in ORR.[11] If this relationship holds, then Figure 3 shows at glance that non-magnetic $Pt_3Y(111)$ adsorbs O* atoms too strongly to be catalytically valuable in ORR. It is also worth to mention that $Pt_3Y(111)$ is the only alloy within the examined pool that shows formation of Pt_3Y-O oxide in the inner layers of the slabs, in agreement with recent experimental results.[12]

On the other hand, following the logic, the series constituted by *3d*-transition metal $Pt_3M(111)$ displays milder chemisorption than the reference system Pt(111), indicating that these magnetic alloys can be considered as good catalysts for ORR. The trend shown in Figure 3 for $Pt_3M(111)$ alloys may suggest the existence of a correlation between the milder chemisorptions and the magnetic properties of the catalyst. The close connection between heterogeneous catalysis[56] and magnetism at macroscopic level is already known as magneto-catalytic effect.[57] We recently demonstrated the impact of QSEI as an energy term contributing to the stabilization of clean slabs of magnetic $Pt_3Co(111)$ alloy and to the destabilization of chemisorbed oxygen atoms.[20] We are hereby extending the study on the important role of QSEI in influencing the chemisorption trend (thus the catalytic behavior) of magnetic catalysts to other bimetallic Pt-based alloys. Figure 4 shows the results obtained for oxygen chemisorption with each isostructural magnetic and non-magnetic nanostructure as a function of the *d*-metal electronic configuration. As it can be seen the O* adsorption trends are different between the magnetic and the fictitious non-magnetic isostructural nanostructures for all the investigated magnetic alloys. The energy discrepancy corresponds to QSEI contribution, that oscillates between ~0.1 eV and ~0.2 eV for the *3d*-metal Pt_3M systems (almost null differences are seen for Pt_3Y and Pt).

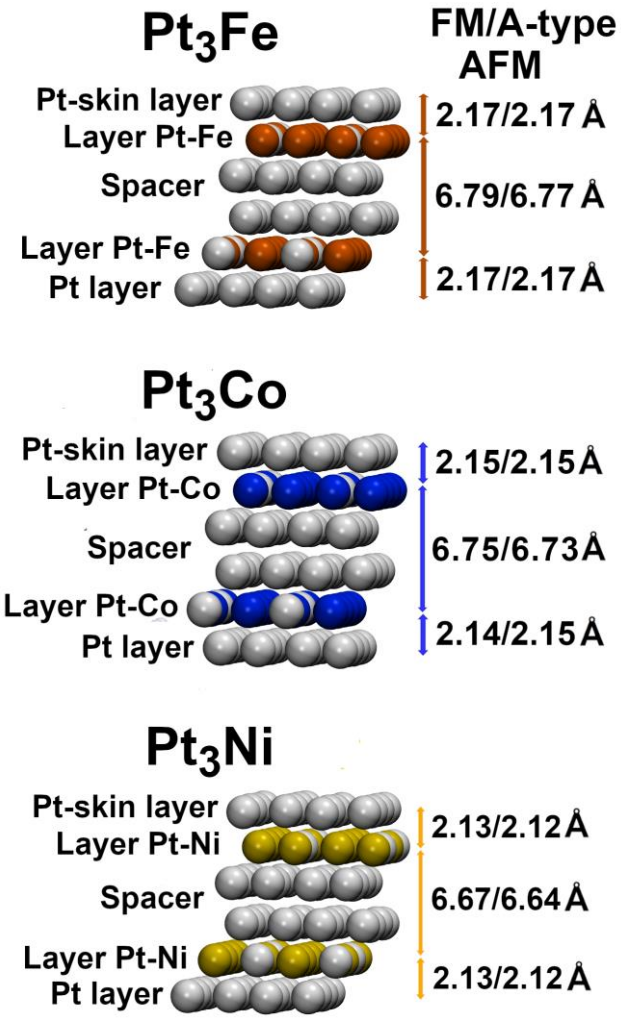

Figure 2. Multi-layered organization of the most stable $Pt_3Fe(111)$, $Pt_3Co(111)$ and $Pt_3Ni(111)$ nanostructures with estimated distances (in Å) between the layers for the FM (right) and A-type AFM (left) orderings, respectively.

Figure 4 also highlights a divergent behavior between Pt_3V, Pt_3Cr, Pt_3Mn and Pt_3Fe, Pt_3Co, Pt_3Ni. The absence of spin terms in the wave functions for fictitious non-magnetic Pt_3V, Pt_3Cr and Pt_3Mn leads to weaker O* bonding predictions than the corresponding isostructural magnetic nanostructures. The absence of spin terms leads instead to a reverse trend for Pt_3Fe, Pt_3Co and Pt_3Ni, showing that the non-magnetic nano-slabs adsorb O* atoms tighter than the corresponding isostructural magnetic ones. Such different trend between spin polarized and non-spin polarized O* chemisorption is explained through the energetic contributions defined in Eq.1.[30]

$$\Delta H_{cat} = \Delta T_{e^-}^{kinetic} + \Delta V_{N+e^-}^{Coulomb} + \Delta V_{e^- - e^-}^{Coulomb} + \Delta QSEI + \\ + \Delta E_{e^-}^{correlation} \quad (1)$$

In the case of non-magnetic close-shell configurations such as $Pt_3Y(111)$ and Pt(111), paired electrons are maximum and share efficiently the inter-nuclear regions between the atoms

(Fermi heaps), hence the influence of QSEI is minimum on ΔH_{cat}, indicating that differentiating spin terms is not essential to reproduce a reliable model of the reactivity of close-shell catalysts. Such description is typically valid for heavier transition metals as well, where *4d* and *5d* orbitals possess larger radial extensions than *3d* and *4f* orbitals due to weak on-site electronic repulsions. Accordingly, the fictitious non-magnetic *3d*-metal Pt_3M nanostructures are assumed as close-shell configurations, hence their behavior can be simply rationalized through chemical effects, as demonstrated in previously published studies on $Pt_3Co(111)$.[20]

On the other hand, the presence of spin polarization in the calculations involving open-shell *3d*-metal $Pt_3M(111)$ series provides additional energetic contributions that leads to different O* chemisorption values depending on the magnetic ordering of the catalyst (Figure 4). Pt_3V, Pt_3Cr and Pt_3Mn bind O* atoms more strongly upon inclusion of spin polarization. These three alloys possess AFM orderings, that induce strong QSEI localized within the *3d* open-shells and a concomitant reduction of the on-site QSEI term ($\Delta QSEI_{on-site}$) (Eq.2).[30]

$$\Delta QSEI = \Delta QSEI_{on-site} + \Delta QSEI_{inter-atomic} \quad (2)$$

Decreased electronic repulsions shortens the *3d*-orbitals radial extension,[58] preventing conductivity through ***interatomic AFM pair localization***. Dominant intra-atomic QSEI in the *3d*-orbitals and optimal inter-atomic nuclei attractions due to the AFM bonds, provide an extra stabilization to high-spin $3d^5$ manganese and chromium. The outcome is a larger energy gap between the $3d_\alpha^5$ occupied bonding orbitals (the Lower Hubbard band) and the $3d_\beta^5$ empty antibonding orbitals (the Upper Hubbard band) of Mn and Cr atoms.[34] This converts $Pt_3Mn(111)$ and $Pt_3Cr(111)$ in more inert catalysts (Figure 3 and 4) compared with FM compositions, as experiments also confirm.[2] G-type AFM $Pt_3V(111)$ presents more favorable O*-chemisorption (Figure 3), but in this case the electron pairs localization typical of AFM compositions and stability issues will yield to high activation barriers for ORR.[27,33]

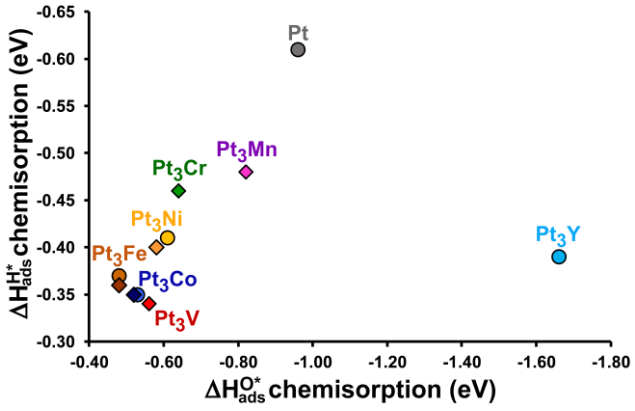

Figure 3. H* versus O* chemisorption trend (in eV for 0.5 ML coverage of adsorbates) onto the most stable nanostructure found for each Pt_3M (M = V, Cr, Mn, Fe, Co, Ni and Y) (111) bimetallic alloy. Diamonds correspond to the chemisorption values for G-type Pt_3V, C-type AFM Pt_3Cr, G-type AFM Pt_3Mn, A-type AFM Pt_3Fe, A-type AFM Pt_3Co and A-type AFM Pt_3Ni. Circles correspond to chemisorption values for FM Pt_3Fe, FM Pt_3Co, FM Pt_3Ni, non-magnetic Pt_3Y and Pt(111) (Pt used as reference). Atomic charge distributions and magnetic contributions per layer are reported in SI pp. S12-S17, S25-S30, S41-S46, S56-S67, S77-S88, S97-S99, S101-S104 and S126-S133.

A different situation concerns FM alloys, such as Pt_3Fe, Pt_3Co and Pt_3Ni, where the inclusion of spin polarization produces milder chemisorption values than the isostructural non-magnetic alloys (Figure 4). In these alloys the FM couplings, mediated by the correlated itinerant electrons, leads to an overall polarization of the electrons in the conduction band. This electronic spin-polarization decreases the adsorption of reaction intermediates affecting, therefore, the chemisorption process.[32] The distance between one spin-electron and another with the same orientation is maximized in FM orderings, generating the so-called Fermi holes; the decrement of the pair localization reduces the electronic repulsions producing a more energetically stable situation (the higher the number of Fermi holes in the FM material, the higher the reduction of electronic repulsions in the valence band and therefore the higher the stabilization carried out by QSEI). FM materials containing Fe, Co and Ni are also known to possess specific conductivity behaviors and transport properties.[21, 44] Experimental results confirm their good performance in ORR,[1-3,5] in photosynthesis[59] and in ammonia synthesis.[33] The difference in chemisorptions seen in Figure 4 for FM Pt_3Fe, Pt_3Co and Pt_3Ni with respect to non-magnetic isostructural slabs, about ~0.2 eV, corresponds indeed to the QSEI contribution in stabilizing the clean slabs, thus concomitantly destabilizing the O*-adsorption.

Interestingly, we calculated that the energy destabilization of the chemisorption introduced by QSEI, Δ= 0.16 eV, 0.23 eV, 0.19 eV for A-type AFM $Pt_3Fe(111)$, $Pt_3Co(111)$ and $Pt_3Ni(111)$, respectively, closely mirrors the QSEI destabilization seen for the corresponding FM alloys reported in Figure 4 (versus non-magnetic structures). A-type AFM Pt_3M (M= Fe, Co, Ni)(111) possess milder H* and O* chemisorption values than C-type AFM Pt_3Cr and G-type AFM Pt_3Mn. This is not serendipitous, however, but in full agreement with previous results indicating that layered antiferromagnetism (A-type) is probability the most active AFM configuration in catalysis.[20, 60] In A-type AFM configurations, QSEI provide dominant ferromagnetic stabilization within the planes of a magnetic layers, but two magnetic layers interact with each other through an antiferromagnetic coupling. The oscillations with the orbital occupancy in Figure 3 also indicate that the *d*-band approximation is not precise for magnetic compositions based on *3d*-metals, where catalytic properties must be analyzed considering all the relevant quantum potentials. A complete theory of the electronic factors in (electro-) catalysis must include the specific quantum description of the relevant electronic correlations.

Figure 4 reinforces the statement previously made for magnetic $Pt_3Co(111)$[20] and extends it to the other *3d*-transition metal $Pt_3M(111)$ alloys: the study of chemical effects alone is not enough to fully describe the chemisorption properties of magnetic catalysts. Cooperative QSEI associated to open-shells have a huge footprint on the complex magnetic and electronic properties reported for *3d*-based highly-correlated materials, where several magnetic centers are linked together by covalent bonds.[20, 31]

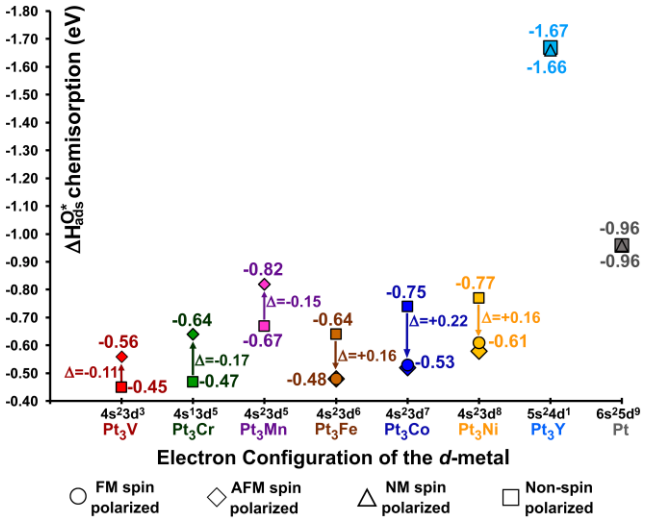

Figure 4. O*-chemisorption trend (in eV) as a function of the *d*-metal electronic configuration for the isostructural magnetic and non-magnetic (NM) slabs of each most stable Pt_3M (M= V, Cr, Mn, Fe, Co, Ni and Y)(111) nanostructure. Δ is the difference between calculated spin polarized and non-spin polarized chemisorptions. Squares correspond to non-magnetic structures, diamonds correspond to AFM structures and circles correspond to FM Pt_3Fe, FM Pt_3Co and FM Pt_3Ni. Triangles correspond to non-magnetic structures treated with spin polarization.

Segregation study on *3d*-transition metal Pt-based alloys. Two main requirements should be fulfilled for a catalyst to be employed in fuel cells (i.e. PEMFCs): binding of transient species (e.g. H* and O*) onto the catalytic surface in the "right" range of strength (too strong or too weak binding energies might limit the catalytic process)[45] and stability of the catalyst throughout every catalytic cycle.[46, 61] It goes without saying that a catalyst with a stable solid structure ensures the preservation of its catalytic activity and durability under the FC operating conditions.[46, 61]

In bimetallic solid compositions one of the main causes of the loss of catalytic activity is represented by the migration of heteroatoms from the sub-layers (usually the sub-skin) to the surface. This phenomenon is known as segregation and it changes the surface composition and electrochemical properties of the catalyst.[46,61] Different factors induce the segregation of the heteroatoms: the subsurface atomic structure, the size and the coordination number of the heterometals, the surface energy and the presence of adsorbed species like O*, OH* and H_2O*.[61-62] The surface energy and the atomic radii are decisive factors for the surface segregation in vacuum.[62]

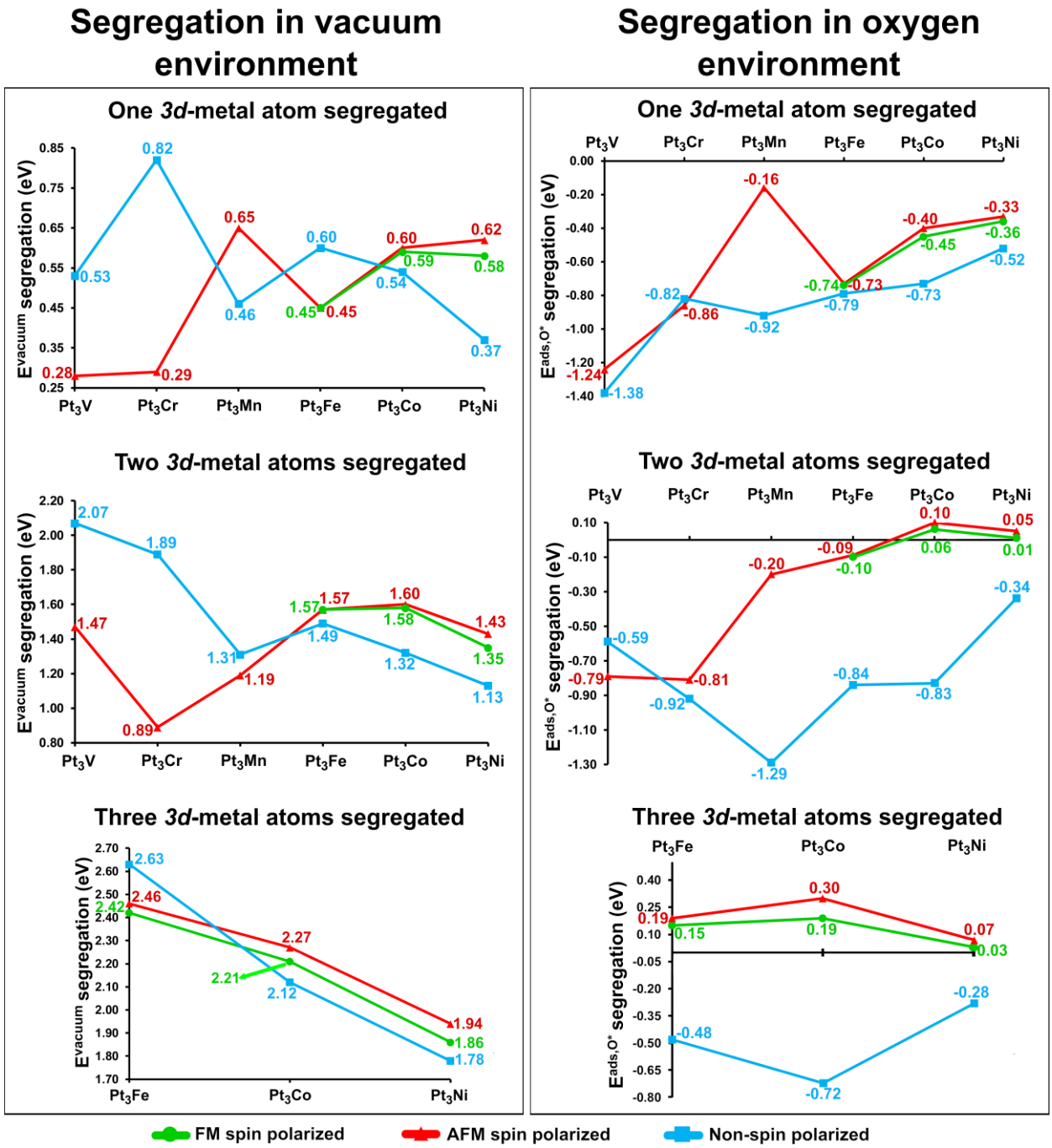

Figure 5. Calculated single-, double- and triple-segregation energies (in eV) under vacuum (left) and under oxygen-adsorption environments (O coverage at 0.5ML) (right) versus $Pt_3M(111)$ species. Straight lines have no physical meaning, rather they are a tool to improve trend visualization.

On the other hand, in the presence of adsorbed species, such as oxygen atoms, the stabilization of the catalytic structure is influenced by the forces involved in the adsorption process, that can or cannot promote the atomic exchange process.[62] Moreover, the segregation of magnetic *3d*-transition metals can be influenced by further important factors, above all the magnetic properties.[62-63] We carried out a computational thermodynamic investigation on segregation of heterometals under vacuum and oxygen-adsorbed environments for the most stable *3d*-metal $Pt_3M(111)$ nanostructures found in our previous structural study presented in Figure 1. We decided to skip the calculations on the segregation of Y atoms in the non-magnetic $Pt_3Y(111)$ alloy since the global minimum presents an erratic pattern with O* atoms embedded into the slab structure itself.

The segregation energies in vacuum are calculated as the difference between the energy of the segregated and the corresponding non-segregated nanostructures, (Eq. 3):[62]

$$E_{segregation}^{vacuum} = E_{segr}^{clean.slab} - E_{non-segr}^{clean.slab} \quad (3)$$

The segregation energies under oxygen-adsorbed environment are obtained as the sum between the segregation energy under vacuum condition and the difference between the adsorption enthalpies of the segregated and non-segregated systems, (Eq.4):[62]

$$E_{segregation}^{ads,O^*} = E_{segregation}^{vacuum} + \left(\Delta H_{segr}^{ads,O^*} - \Delta H_{non-segr}^{ads,O^*}\right) \quad (4)$$

In accordance with the purposes and the philosophy of this manuscript, this study aimed also to include the role of magnetism and QSEI in the segregation process, by running spin polarized and non-spin polarized calculations on isostructural *3d*-segregated and non-segregated *3d*-metal nanostructures. Figure 5 displays the results of the segregation study for up-to-three *3d*-metals in vacuum (left) and with O* (right). The segregation energies in vacuum ($E_{segregation}^{vacuum}$, via Eq. 3) display positive values for both isostructural spin and non-spin polarized calculations (Figure 5, left). Positive $E_{segregation}^{vacuum}$ values indicates that the segregation of *3d*-metals is not thermodynamically favored in all the most stable clean Pt_3M (M= V, Cr, Mn, Fe, Co, Ni)(111) alloys. This confirms that the Pt-skin configuration is the most thermodynamically stable atomic arrangement under vacuum for these bimetallic alloys, in excellent agreement with experimental and computational data.[62,64] Nonetheless, remarkably interesting differences are observed between isostructural spin polarized and non-spin polarized $E_{segregation}^{vacuum}$. For instance, the trend of non-spin polarized series suggests that $Pt_3V(111)$ and $Pt_3Cr(111)$ are the most thermodynamically stable alloys against the segregation process, while the spin polarized trend points at $Pt_3Co(111)$ and $Pt_3Ni(111)$ alloys as the less prone to the *3d*-segregation in vacuum. Thus, the exclusion of spin terms in $Pt_3V(111)$ and $Pt_3Cr(111)$ greatly overestimates $E_{segregation}^{vacuum}$. For instance, $E_{segregation}^{vacuum}$ for the segregation of one Cr atom in the fictitious non-magnetic Pt_3Cr is 0.82 eV, when $E_{segregation}^{vacuum}$ is 0.29 eV in the realistic C-type AFM Pt_3Cr (0.53 eV lower!), due to the presence of the spin polarization. On the contrary, an opposite trend is observed for magnetic $Pt_3Co(111)$ and $Pt_3Ni(111)$. For example, the segregation of one Ni atom results more thermodynamically disfavored in FM Pt_3Ni (0.58 eV) than in the hypothetical isostructural non-magnetic nanostructure (0.37 eV). In this latter case QSEI contribute to thermodynamically stabilize the Pt-skin configuration of FM Pt_3Ni by a non-negligible 0.21 eV. It is also very important to mention that the exclusion of spin polarization can also lead to different atomic dispositions. Remarkably, non-spin polarized calculations for the segregation of one Mn atom in $Pt_3Mn(111)$ alloy provide a lowest energy segregated nanostructure structurally different from the one provided by the inclusion of spin polarization (see SI pp. S110- S111).

Similar discrepancies are observed in Figure 5, right, between spin and non-spin polarized calculations in the oxygen-induced segregation energies, ($E_{segregation}^{ads,O^*}$ via Eq. 4). $E_{segregation}^{ads,O^*}$ is a combination of the contribution of the segregation energy in vacuum ($E_{segregation}^{vacuum}$) and the contribution of the difference between the O*-adsorption on the *3d*-segregated ($\Delta H_{segr}^{ads,O^*}$) and on the initial non-segregated nanostructures ($\Delta H_{non-segr}^{ads,O^*}$) (see SI pp. S118-S120). $E_{segregation}^{ads,O^*} < 0$ is obtained when ($\Delta H_{segr}^{ads,O^*} - \Delta H_{non-segr}^{ads,O^*}$) term prevails on $E_{segregation}^{vacuum}$ contribution, thus favoring segregation, vice versa, when $E_{segregation}^{ads,O^*} > 0$ is obtained, the segregation is disfavored. In the latter case, the Pt-skin configuration of the nanostructures results to be thermodynamically stable enough to prevent the segregation process when O* atoms are adsorbed onto the surface. Figure 5, right, shows that G-type $Pt_3V(111)$ and C-type $Pt_3Cr(111)$ alloys generally exhibit the most negative $E_{segregation}^{ads,O^*}$ values. For instance, $E_{segregation}^{ads,O^*}$ is -1.24 eV for a mono-segregation of V onto the surface. Positive values, $E_{segregation}^{ads,O^*} > 0$, are only obtained for the spin polarized calculations of magnetic $Pt_3Co(111)$ and $Pt_3Ni(111)$, when double- and triple-segregations take place (e.g. two or three segregated atoms onto the surface). For instance, $E_{segregation}^{ads,O^*}$ values for A-type AFM Pt_3Co are 0.10 eV and 0.30 eV when two and three Co atoms segregate to the surface, respectively. Magnetic $Pt_3Fe(111)$ represents an exception in the series, since a positive $E_{segregation}^{ads,O^*}$ is only observed when all the three Fe metals are exchanged to the surface.

Figure 3 shows that the trend in O*-chemisorption with non-segregated slabs increases along the period, with FM $Pt_3Fe(111)$, -0.48 eV, < FM $Pt_3Co(111)$, -0.53 eV, < FM $Pt_3Ni(111)$, -0.61 eV, but, most interestingly, the chemisorption trend for the mono-segregated slabs is completely reversed, with FM $Pt_3Fe(111)$, -1.67 eV, > FM $Pt_3Co(111)$, -1.57 eV, > FM $Pt_3Ni(111)$, -1.56 eV (this also stands true for double- and triple-segregations, see SI pp. S118-S120). These data, showing mild chemisorptions and good resilience to segregation, suggest unequivocally that magnetic $Pt_3Co(111)$ are definitely a good catalytic choice in fuel cells at present times and, more importantly, that multilayered magnetic $Pt_3Fe(111)$ might become an even better choice, once the stability issues are completely resolved (the strong affinity of Fe for oxygen leads to stronger binding with the surface and easier segregation of the Fe atoms). Recent experiments strongly support our computational results proving that magnetic PtFe nanoparticles, composed by consecutive layers of Pt and Fe atoms, exhibit an enhanced ORR catalytic activity and a higher durability than the commercial Pt/C catalyst upon doping with Au atoms.[65]

For comparison, the exclusion of the spin polarization produces thermodynamically favored *3d*-segregations for all the investigated cases. The cases of $Pt_3Co(111)$ and $Pt_3Ni(111)$ are outstanding, since the calculations in absence of spin terms predict a completely opposite trend for double- and triple-segregations compared to spin polarized calculations. For instance, $E_{segregation}^{ads,O^*} > 0$ (0.30 eV and 0.19 eV for A-type AFM and FM Pt_3Co, respectively) is found for triple-segregation of Co atoms when the spin polarization is included in the calculations, while, in absence of spin polarization, $E_{segregation}^{ads,O^*}$ = -0.72 eV indicates instead a thermodynamically feasible process. Two considerations are essential at this point: it is evident that QSEI plays a central role in the stabilization of magnetic nanostructures (this is especially true for magnetic $Pt_3Fe(111)$, $Pt_3Co(111)$ and $Pt_3Ni(111)$) and that the exclusion of spin polarization from the calculations of strongly-correlated models leads to unphysical artifacts.

Since Pt_3Fe, Pt_3Co and Pt_3Ni show good resistance towards the segregation of magnetic atoms, it is reasonable to believe that their layered arrangements provide a certain degree of inertia toward segregation. Indeed, the comparison with other less ordered *3d*-metal distributions for these three alloys (e.g., these distributions resemble more closely a single-phase than the layered structures) shows that the structural benefit of the multilayered arrangement provides an overall thermodynamic stabilization toward the degradation of the catalytic structure both under vacuum and oxygen environments (see SI pp. S121-S126).

Figure 6 correlates the segregation in FM and A-AFM O*-adsorbed $Pt_3Co(111)$ nanostructures with the length and magnetization of the non-magnetic Pt-spacer (3rd and 4th layers).

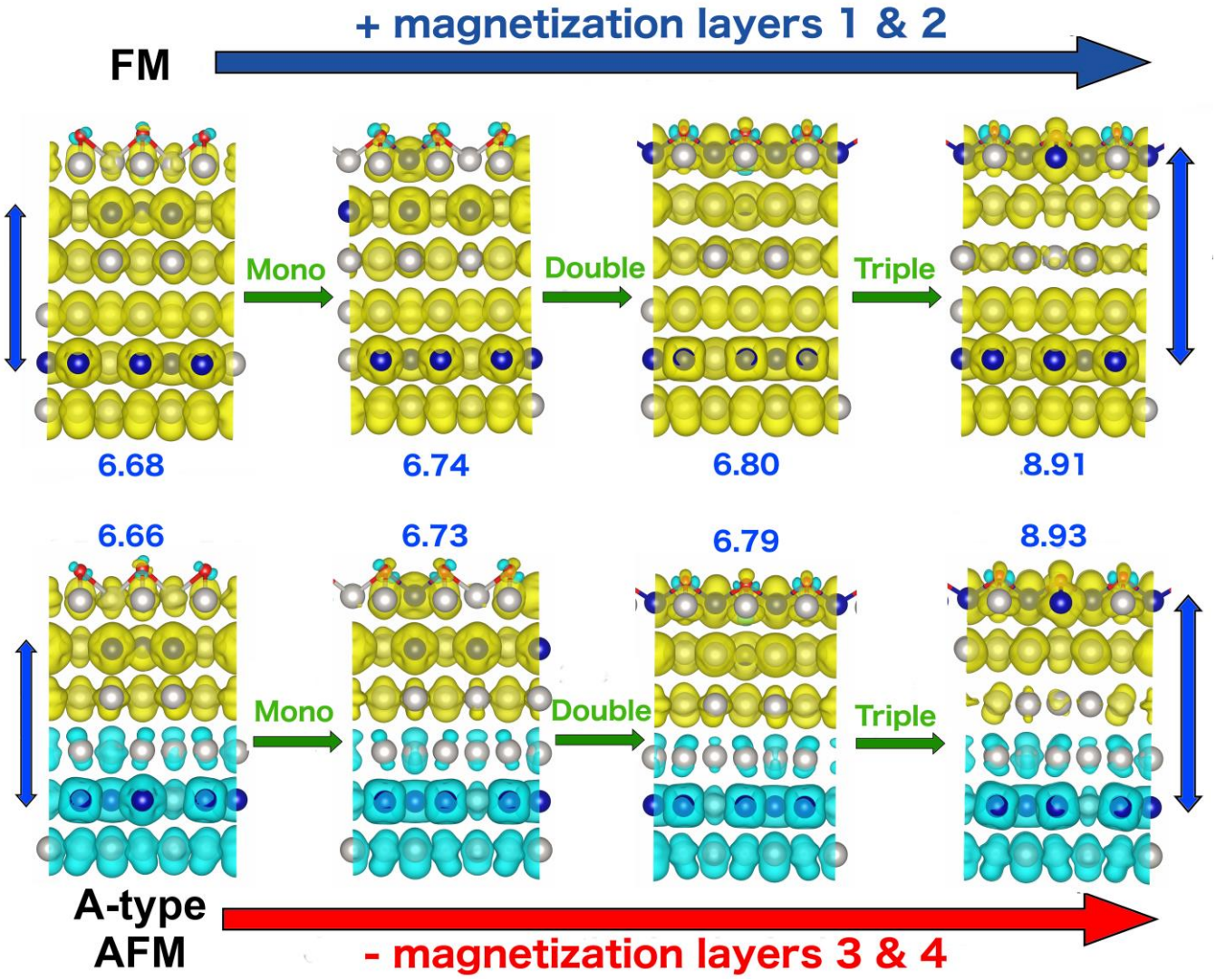

Figure 6. Pt-spacer length (Å, in blue) and spin density plots for non-, mono-, double- and triple-segregated FM and A-type AFM $Pt_3Co(111)$ nanostructures (from left to right). The yellow and cyan isosurfaces (0.004 a_0^{-3}, where a_0 is Bohr radius) represents spin-up and spin-down polarizations, respectively. Pt, Co and O atoms are colored in grey, blue and red, respectively.

Figure 6 shows that the mono-segregation of Co atoms from the magnetically active 2nd layer in $Pt_3Co(111)$ weakens, but does not completely destroy, the layered structure; this mono-segregation is, in fact, exothermic with $E_{segregation}^{ads,O^*}$ = -0.45 and -0.40 eV for FM and AFM structures, respectively. The polarization of the non-magnetic spacer (3rd and 4th layers) decreases slightly from the clean structure (Figure 6, first step). The double-segregation weakens ulteriorly the layered structure (only one Co is left in the 2nd layer now) and the polarization of the Pt-spacer visibly decays further from the mono-segregated case (Figure 6, second step). This further disruption of the original cooperative layered structure is strongly antagonized, however, and the second exchange is thermodynamically disfavored ($E_{segregation}^{ads,O^*}$ = 0.06 and 0.10 eV for FM and AFM structures, respectively). When all the three Co atoms are segregated to the surface ($E_{segregation}^{ads,O^*}$ = 0.19 and 0.30 eV for FM and AFM structures, respectively), the original layered structure with ~6.7 Å Pt-spacer is destroyed, forming a new layered structure with ~8.9 Å Pt-spacer: the increment of the length of the Pt-spacer (three-layers wide now) leads to a concomitant decrement of spin polarization in the spacer, clearly observable in Figure 6, third step (the A-type AFM ordering only loses polarization on the 3rd layer). The increment of the spacer length in multilayered Pt/Co structures is known experimentally to influence the effectiveness of the interlayer exchange coupling, affecting the transfer of magnetic information among the FM layers.[48] Similar trends are obtained for FM and A-AFM $Pt_3Fe(111)$ and A-AFM $Pt_3Ni(111)$ nanostructures; the decrement of the polarization of the Pt-spacers qualitatively follows the thermodynamic trend seen for the segregations (the loss of polarization in the spacer is milder in Pt_3Fe, but seems to be severe for Pt_3Ni, see SI pp. S112-S117). We think that the magnetism effects provide thermodynamic stability to these nanostructures. Our claim is even more amplified if we consider the completely opposite trend shown by fictitious non-magnetic $Pt_3Fe(111)$, $Pt_3Co(111)$ and

$Pt_3Ni(111)$ for the segregation in Figure 5: the complete absence of magnetic effects, while retaining unchanged ligand, strain and ensemble effects (the fictitious non-magnetic nanostructures are isostructural with the magnetic ones), leads to strongly exothermic mono-, double- and triple-segregation for all the three alloys. Under this perspective, then, each catalytic event is not only structurally and energetically influenced by the surface properties of the solid catalyst, but also by the whole catalytic structure.[56]

CONCLUSIONS

This work proposes a detailed computational study on *d*-transition metal Pt based alloys, Pt_3M (M= V, Cr, Mn, Fe, Co, Ni and Y)(111), from their structural organization to oxygen chemisorption capabilities and resistance against segregation of subskin magnetic atoms. The aim of the study clearly lies in proposing theoretical models as synthetic targets. A speciation to identify the most stable *3d*-metal distribution within the theoretical slabs has been carried out and multilayered structures have been found to be the most stable structures for Pt_3M (M = Fe, Co, Ni).

The intriguing multilayered structure (two magnetic layers separated by a non-magnetic spacer), probably unusual in the context of heterogeneous catalysis, but very popular in the fields of spintronics and solid-state devices, is a global minimum in the structural organization of $Pt_3Fe(111)$, $Pt_3Co(111)$ and $Pt_3Ni(111)$ alloys. Such magnetic layered structural organization enables catalytically favorable chemisorption of H* and O* atoms and partially hampers migration of sub-skin magnetic atoms onto the solid surface (segregation), compared to all the other $Pt_3M(111)$ alloys in this study.

Our *a priori* calculations suggest that magnetic multilayered $Pt_3Fe(111)$, $Pt_3Co(111)$ and $Pt_3Ni(111)$ nanostructures fulfill the catalytic requirements of optimal behavior and some stability resulting to be, as we know, the actual candidates for fuel cells. Despite the inherently difficult synthetic challenge of obtaining a monoatomic layer of pure metals or alloys, ultrathin layers, composed by few monoatomic layers, closely resembling our theoretical model, are accessible *via* magnetron sputtering.[66] Multilayered systems have been synthesized by physicists tuning magnetic and structural interplay between the layers (e.g. thickness of the layers, the size and the type of materials).[67] Pt_3Ni displays the best level of structural stability, but stronger chemisorption of transient species. Pt_3Co satisfies both the criteria of stability against segregation and mild chemisorption of species. $Pt_3Fe(111)$ possesses very low chemisorption of transient species and, after resolution of its stability issues towards oxygen, may become an excellent catalytic choice, as strongly confirmed independently by recent experimental studies on Au-doped PtFe nanoparticles.[65]

The rational design of optimal catalysts based on abundant and cheap *3d*-metals for the production of clean energy in PEMFCs cannot be achieved without a deep understanding of the electronic structure-catalytic activity correlation,[57] where magnetism plays a fundamental role. This work demonstrates that structure, quantum spin exchange interactions (QSEI) and chemisorption properties (thus catalytic activity) are subtly connected one another. The inclusion of spin terms into the calculations of bimetallic $Pt_3M(111)$ alloys (and in general of magnetic catalysts based on *3d*-metals) is a *conditio sine qua non* a comprehensive and correct description of physical and chemical properties of the material cannot be achieved. In plain terms, QSEI allow the electrons with the same spin to have (the actual) quantum mechanisms to run away from each other, reducing their mutual repulsion. Such mechanism yield to the concept of FM enhanced nobility: milder chemisorption values and spin-mobility.

COMPUTATIONAL METHODS

The study was performed by periodic Density Functional Theory (DFT) calculations using VASP.[68-71] The exchange-correlation energy was calculated within the generalized gradient approximation using the Perdew-Burke-Ernzerhof functional revised for solids (PBEsol).[72] The DFT+U approach was applied to account for the strong correlation among the electrons in the *3d*-metals (U = 2-3).[73] The electron-ion interactions for the atoms were described by the projector augmented wave method developed by Blöchl.[74-75] For the expansion of the wave function into the plane wave, the cut-off energy was set at 400 eV. The Monkhorst–Pack scheme was chosen for the integration in the reciprocal space.[76] Every Pt_3M slab model was made of 6 metallic layers in 2x2 unit cells and about 15 Å vacuum gap. The optimized lattice parameters are the following: for $Pt_3Co(111)$, $Pt_3Ni(111)$ and $Pt_3Fe(111)$ close-packed surfaces a = 23.6-23.8 Å, b ~ 5.4 Å and c ~ 4.5 Å; for $Pt_3Cr(111)$ and $Pt_3V(111)$ close-packed surfaces a = ~23.3 Å, b ~ 5.4 Å and c ~ 4.6 Å; for $Pt_3Mn(111)$ close-packed surfaces a ~ 23.2-23.3 Å, b ~ 5.5 Å and c ~ 4.5 Å; for $Pt_3Y(111)$ close-packed surfaces a ~ 22.3 Å, b ~ 5.2 Å and c ~ 5.0 Å. The reciprocal space was sampled with a (1x7x7) k-point grid for all the investigated alloys. The segregation model was built by exchanging the positions of the Pt atoms on the surface with the underneath *3d*-metal atoms within the most stable nanostructure with O-coverage at 0.5 ML found for each alloy: a maximum double segregation was considered for $Pt_3V(111)$, $Pt_3Cr(111)$ and $Pt_3Mn(111)$ (the 2nd layer contains only 50 % of *3d*-metal) and a maximum triple segregation was considered for $Pt_3Fe(111)$, $Pt_3Co(111)$ and $Pt_3Ni(111)$ (the 2nd layer contains only 75 % of *3d*-metal). We calculated the segregation energies using the reported method in literature (see SI for further details).[62] As customary in the field, the computational studies presented in this article were carried out at 0 K. Bringing the model up to the working temperatures of modern fuel cells needs the inclusion of the thermal expansion of the unit cell and a substantial amount of thermal corrections to the electronic energy and entropy that are outside of the scope of the present work.

ASSOCIATED CONTENT

Supporting Information

DFT calculations, chemisorption study, Bader charge analysis and magnetic moments, spin density plots, adsorbed nanostructures, calculated *d*-band center, Pt-spacer magnetization comparison between Pt_3M (M= Fe, Co, Ni) (111) alloys, structural effects of the multilayered structures and segregation study (slab models and data set).

AUTHOR INFORMATION

Corresponding Author

*Jose Gracia, E-mail: magnetocat@outlook.com

Author Contributions

The manuscript was written through contributions of all authors.

Notes

The authors declare no competing financial interest.

ACKNOWLEDGMENT

C.B. and J.G. thank Prof. Armando Beltrán Flors (Quimica Teorica y Computacional) and the Servei D'Informatica of the University Jaume I for the provision ofthe facilities employed in this work. The resources from the supercomputer "Memento", technical expertise and assistance provided by BIFI-ZCAM (Universidad de Zaragoza) are acknowledged. MF gratefully acknowledges Prof. M.A. Perìcas and ICIQ to support his postdoctoral position. VP gratefully acknowledges the financial support from the Spanish Ministerio de Economía y Competitividad (MINECO/FEDER) under the Project PGC2018-099383-B-I00.

REFERENCES

(1) Kim, C.; Dionigi, F.; Beermann, V.; Wang, X.; Möller, T.; Strasser, P., Alloy Nanocatalysts for the Electrochemical Oxygen Reduction (ORR) and the Direct Electrochemical Carbon Dioxide Reduction Reaction (CO_2RR). *Adv. Mater.* **2019**, *31* (31), 1805617.

(2) Stamenkovic, V. R.; Mun, B. S.; Arenz, M.; Mayrhofer, K. J. J.; Lucas, C. A.; Wang, G.; Ross, P. N.; Markovic, N. M., Trends in Electrocatalysis on Extended and Nanoscale Pt-Bimetallic Alloy Surfaces. *Nat. Mater.* **2007**, *6* (3), 241-247.

(3) Stamenkovic, V.; Mun, B. S.; Mayrhofer, K. J. J.; Ross, P. N.; Markovic, N. M.; Rossmeisl, J.; Greeley, J.; Nørskov, J. K., Changing the Activity of Electrocatalysts for Oxygen Reduction by Tuning the Surface Electronic Structure. *Angew. Chem. Int. Ed.* **2006**, *45* (18), 2897-2901.

(4) Sui, S.; Wang, X.; Zhou, X.; Su, Y.; Riffat, S.; Liu, C.-j., A comprehensive review of Pt electrocatalysts for the oxygen reduction reaction: Nanostructure, Activity, Mechanism and Carbon Support in PEM Fuel Cells. *J. Mater. Chem. A* **2017**, 5 (5), 1808-1825.

(5) Toda, T., Enhancement of the Electroreduction of Oxygen on Pt Alloys with Fe, Ni, and Co. *J. Electrochem. Soc.* **1999**, *146* (10), 3750-3756.

(6) Stamenkovic, V. R.; Fowler, B.; Mun, B. S.; Wang, G.; Ross, P. N.; Lucas, C. A.; Marković, N. M., Improved Oxygen Reduction Activity on $Pt_3Ni(111)$ via Increased Surface Site Availability. *Science* **2007**, *315* (5811), 493-497.

(7) Wang, Y.-H.; Le, J.-B.; Li, W.-Q.; Wei, J.; Radjenovic, P. M.; Zhang, H.; Zhou, X.-S.; Cheng, J.; Tian, Z.-Q.; Li, J.-F., In situ Spectroscopic Insight into the Origin of the Enhanced Performance of Bimetallic Nanocatalysts towards the Oxygen Reduction Reaction (ORR). *Angew. Chem. Int. Ed.* **2019**, *58* (45), 16062-16066.

(8) Cui, Z.; Chen, H.; Zhou, W.; Zhao, M.; DiSalvo, F. J., Structurally Ordered Pt_3Cr as Oxygen Reduction Electrocatalyst: Ordering Control and Origin of Enhanced Stability. *Chem. Mater.* **2015**, *27* (21), 7538-7545.

(9) Zou, L.; Li, J.; Yuan, T.; Zhou, Y.; Li, X.; Yang, H., Structural Transformation of Carbon-Supported Pt_3Cr Nanoparticles from a Disordered to an Ordered Phase as a Durable Oxygen Reduction Electrocatalyst. *Nanoscale* **2014**, *6* (18), 10686-10692.

(10) Gallego, S.; Ocal, C.; Muñoz, M. C.; Soria, F., Surface-Layered Ordered Alloy (Pt/Pt_3Mn) on Pt(111). *Phys. Rev. B* **1997**, *56* (19), 12139-12142.

(11) Greeley, J.; Stephens, I. E. L.; Bondarenko, A. S.; Johansson, T. P.; Hansen, H. A.; Jaramillo, T. F.; Rossmeisl, J.; Chorkendorff, I.; Nørskov, J. K., Alloys of Platinum and Early Transition Metals as Oxygen Reduction Electrocatalysts. *Nat. Chem.* **2009**, *1* (7), 552-556.

(12) Brown, R.; Vorokhta, M.; Khalakhan, I.; Dopita, M.; Vonderach, T.; Skála, T.; Lindahl, N.; Matolínová, I.; Grönbeck, H.; Neyman, K. M.; Matolín, V.; Wickman, B., Unraveling the Surface Chemistry and Structure in Highly Active Sputtered Pt_3Y Catalyst Films for the Oxygen Reduction Reaction. *ACS Appl. Mater. Inter.* **2020**, *12* (4), 4454-4462.

(13) Rodriguez, J. A.; Goodman, D. W., Surface Science Studies of the Electronic and Chemical Properties of Bimetallic Systems. *J. Phys. Chem.* **1991**, *95* (11), 4196-4206.

(14) Kitchin, J. R.; Nørskov, J. K.; Barteau, M. A.; Chen, J. G., Modification of the Surface Electronic and Chemical Properties of Pt(111) by Subsurface 3d-Transition Metals. *J. Chem. Phys.* **2004**, *120* (21), 10240-10246.

(15) Bligaard, T.; Nørskov, J. K., Ligand Effects in Heterogeneous Catalysis and Electrochemistry. *Electrochim. Acta* **2007**, *52* (18), 5512-5516.

(16) Mavrikakis, M.; Hammer, B.; Nørskov, J. K., Effect of Strain on the Reactivity of Metal Surfaces. *Phys. Rev. Lett.* **1998**, *81* (13), 2819-2822.

(17) Liu, P.; Nørskov, J. K., Ligand and Ensemble Effects in Adsorption on Alloy Surfaces. *Phys. Chem. Chem. Phys.* **2001**, *3* (17), 3814-3818.

(18) Kobayashi, S.; Aoki, M.; Wakisaka, M.; Kawamoto, T.; Shirasaka, R.; Suda, K.; Tryk, D. A.; Inukai, J.; Kondo, T.; Uchida, H., Atomically Flat Pt Skin and Striking Enrichment of Co in Underlying Alloy at $Pt_3Co(111)$ Single Crystal with Unprecedented Activity for the Oxygen Reduction Reaction. *ACS Omega* **2018**, *3* (1), 154-158.

(19) Hu, G.; Gracia-Espino, E.; Sandström, R.; Sharifi, T.; Cheng, S.; Shen, H.; Wang, C.; Guo, S.; Yang, G.; Wågberg, T., Atomistic Understanding of the Origin of High Oxygen Reduction Electrocatalytic Activity of Cuboctahedral Pt_3Co–Pt Core–Shell Nanoparticles. *Catal. Sci. Tech.* **2016**, *6* (5), 1393-1401.

(20) Biz, C.; Fianchini, M.; Gracia, J., Catalysis Meets Spintronics; Spin Potentials Associated with Open-Shell Orbital Configurations Enhance the Activity of Pt_3Co Nanostructures for Oxygen Reduction: A Density Functional Theory Study. *ACS Appl. Nano Mater.* **2020**, *3* (1), 506-515.

(21) Mott, N. F., Electrons in Transition Metals. *Adv. Phys.* **1964**, *13* (51), 325-422.

(22) Ishikawa Y., M. N., Physics and Engineering Applications of Magnetism. Springer-Verlag: **1991**.

(23) Goodenough, J. B., Magnetism and the Chemical Bond. Interscience Publisher-Wiley & Sons: **1963**.

(24) Getzlaff, M., Fundamentals of Magnetism. Springer: **2008**.

(25) J., W. H. P., Magnetic Properties of Metals. d-Element, Alloys and Compounds. Springer-Verlag: **1991**.

(26) Heisenberg, W., Mehrkörperproblem und Resonanz in der Quantenmechanik. *Z. Phys.* **1926**, *38* (6), 411-426.

(27) Gracia, J., Spin Dependent Interactions Catalyse the Oxygen Electrochemistry. *Phys. Chem. Chem. Phys.* **2017**, *19* (31), 20451-20456.

(28) Gracia, J., What Are the Electrons Really Doing in Molecules? A Space-Time Picture. *Eur. J. Phys. Ed.* **2020**, *11* (1), 1-19.

(29) Dirac, P. A. M.; Fowler, R. H., On the Theory of Quantum mechanics. *Proc. R. Soc. London Ser. A* **1926**, *112* (762), 661-677.

(30) Szabo, A. O., N. S., Modern Quantum Chemistry. Introduction to Advanced Electronic Structure Theory. Dover Publications Inc.: **1996**.

(31) Dagotto, E., Complexity in Strongly Correlated Electronic Systems. *Science* **2005**, *309* (5732), 257-262.

(32) Zhang, L.; Cheruvathur, A.; Biz, C.; Fianchini, M.; Gracia, J., Ferromagnetic Ligand Holes in Cobalt Perovskite Electrocatalysts as an Essential Factor for High Activity towards Oxygen Evolution. *Phys. Chem. Chem. Phys.* **2019**, *21* (6), 2977-2983.

(33) Munarriz, J.; Polo, V.; Gracia, J., On the Role of Ferromagnetic Interactions in Highly Active Mo-Based Catalysts for Ammonia Synthesis. *ChemPhysChem* **2018**, *19* (21), 2843-2847.

(34) Gracia, J.; Biz, C.; Fianchini, M., The Trend of Chemisorption of Hydrogen and Oxygen Atoms on Pure Transition Metals: Magnetism Justifies Unexpected Behaviour of Mn and Cr. *Mat.Today Comm.* **2020**, *23*, 100894.

(35) Gracia, J.; Munarriz, J.; Polo, V.; Sharpe, R.; Jiao, Y.; Niemantsverdriet, J. W.; Lim, T., Analysis of the Magnetic Entropy in Oxygen Reduction Reactions Catalysed by Manganite Perovskites. *ChemCatChem* **2017**, *9* (17), 3358-3363.

(36) Sharpe, R.; Lim, T.; Jiao, Y.; Niemantsverdriet, J. W.; Gracia, J., Oxygen Evolution Reaction on Perovskite Electrocatalysts with Localized Spins and Orbital Rotation Symmetry. *ChemCatChem* **2016**, *8* (24), 3762-3768.

(37) Li, X.; Liu, H.; Chen, Z.; Wu, Q.; Yu, Z.; Yang, M.; Wang, X.; Cheng, Z.; Fu, Z.; Lu, Y., Enhancing Oxygen Evolution Efficiency of Multiferroic Oxides by Spintronic and Ferroelectric Polarization Regulation. *Nat. Commun.* **2019**, *10* (1), 1409.

(38) Sun, S.; Sun, Y.; Zhou, Y.; Shen, J.; Mandler, D.; Neumann, R.; Xu, Z. J., Switch of the Rate-Determining Step of Water Oxidation by Spin-Selected Electron Transfer in Spinel Oxides. *Chem. Mater.* **2019**, *31* (19), 8106-8111.

(39) Garcés-Pineda, F. A.; Blasco-Ahicart, M.; Nieto-Castro, D.; López, N.; Galán-Mascarós, J. R., Direct Magnetic Enhancement of Electrocatalytic Water Oxidation in Alkaline Media. *Nat. Energy* **2019**, *4* (6), 519-525.

(40) Zeng, Z.; Zhang, T.; Liu, Y.; Zhang, W.; Yin, Z.; Ji, Z.; Wei, J., Magnetic Field-Enhanced 4-Electron Pathway for Well-Aligned Co_3O_4/Electrospun Carbon Nanofibers in the Oxygen Reduction Reaction. *ChemSusChem* **2018**, *11* (3), 580-588.

(41) Matsushima, H.; Iida, T.; Fukunaka, Y.; Bund, A., PEMFC Performance in a Magnetic Field. *Fuel Cells* **2008**, *8* (1), 33-36.

(42) Westsson, E.; Picken, S.; Koper, G., The Effect of Magnetic Field on Catalytic Properties in Core-Shell Type Particles. *Front. Chem.* **2020**, *8*, 163.

(43) Liu, X.; Li, Y.; Xue, J.; Zhu, W.; Zhang, J.; Yin, Y.; Qin, Y.; Jiao, K.; Du, Q.; Cheng, B.; Zhuang, X.; Li, J.; Guiver, M. D., Magnetic Field Alignment of Stable Proton-Conducting Channels in an Electrolyte Membrane. *Nat. Commun.* **2019**, *10* (1), 842.

(44) Chappert, C.; Fert, A.; Van Dau, F. N., The Emergence of Spin Electronics in Data Storage. *Nat. Mater.* **2007**, *6* (11), 813-823.

(45) Nørskov, J. K.; Bligaard, T.; Logadottir, A.; Bahn, S.; Hansen, L. B.; Bollinger, M.; Bengaard, H.; Hammer, B.; Sljivancanin, Z.; Mavrikakis, M.; Xu, Y.; Dahl, S.; Jacobsen, C. J. H., Universality in Heterogeneous Catalysis. *J. Catal.* **2002**, *209* (2), 275-278.

(46) Bing, Y.; Liu, H.; Zhang, L.; Ghosh, D.; Zhang, J., Nanostructured Pt-Alloy Electrocatalysts for PEM Fuel Cell Oxygen Reduction Reaction. *Chem. Soc. Rev.* **2010**, *39* (6), 2184-2202.

(47) Johnson, M. T.; Bloemen, P. J. H.; Broeder, F. J. A. d.; Vries, J. J. d., Magnetic Anisotropy in Metallic Multilayers. *Rep. Prog. Phys.* **1996**, *59* (11), 1409-1458.

(48) An, Y.; Duan, L.; Liu, T.; Wu, Z.; Liu, J., Structural and Magnetic Properties of Pt in Co/Pt Multilayers. *Appl. Surf. Sci.* **2011**, *257* (17), 7427-7431.

(49) Krishnan, R.; Lassri, H.; Porte, M.; Tessier, M.; Renaudin, P., Perpendicular Magnetization in Ni/Pt Multilayers. *Appl. Phys. Lett.* **1991**, *59* (27), 3649-3650.

(50) Weller, D.; Brändle, H.; Gorman, G.; Lin, C. J.; Notarys, H., Magnetic and Magneto-Optical Properties of Cobalt-Platinum Alloys with Perpendicular Magnetic Anisotropy. *Appl. Phys. Lett.* **1992**, *61* (22), 2726-2728.

(51) Simopoulos, A.; Devlin, E.; Kostikas, A.; Jankowski, A.; Croft, M.; Tsakalakos, T., Structure and Enhanced Magnetization in Fe/Pt Multilayers. *Phys. Rev. B* **1996**, *54* (14), 9931-9941.

(52) Shin, S.-C.; Srinivas, G.; Kim, Y.-S.; Kim, M.-G., Observation of Perpendicular Magnetic Anisotropy in Ni/Pt Multilayers at Room Temperature. *Appl. Phys. Lett.* **1998**, *73* (3), 393-395.

(53) Stiles, M. D., Interlayer Exchange Coupling. *J. Magn. Magn. Mater.* **1999**, *200* (1), 322-337.

(54) Wu, R.; Chen, L.; Kioussis, N., Structural and Magnetic Properties of Fcc Pt/Fe(111) Multilayers. *J. Appl. Phys.* **1996**, *79* (8), 4783-4785.

(55) Trasatti, S., Electrocatalysis by Oxides-Attempt at a Unifying Approach. *J. Electroanal. Chem.*, **1980**, *111*, 125-131.

(56) Balandin, A. A., Modern State of the Multiplet Theor of Heterogeneous Catalysis. In *Advances in Catalysis*, Eley, D. D.; Pines, H.; Weisz, P. B., Eds. Academic Press **1969**; Vol. 19, pp 1-210.

(57) Dowden, D. A., 56. Heterogeneous catalysis. Part I. Theoretical basis. *J. Chem. Soc.* **1950**, (0), 242-265.

(58) Landrum, G. A.; Dronskowski, R., The Orbital Origins of Magnetism: From Atoms to Molecules to Ferromagnetic Alloys. *Angew. Chem. Int. Ed.* **2000**, *39* (9), 1560-1585.

(59) Jiao, Y.; Sharpe, R.; Lim, T.; Niemantsverdriet, J. W. H.; Gracia, J., Photosystem II Acts as a Spin-Controlled Electron Gate during Oxygen Formation and Evolution. *J. Am. Chem. Soc.* **2017**, *139* (46), 16604-16608.

(60) Lim, T.; Niemantsverdriet, J. W.; Gracia, J., Layered Antiferromagnetic Ordering in the Most Active Perovskite Catalysts for the Oxygen Evolution Reaction. *ChemCatChem* **2016**, *8* (18), 2968-2974.

(61) Farsi, L.; Deskins, N. A., First Principles Analysis of Surface Dependent Segregation in Bimetallic Alloys. *Phys. Chem. Chem. Phys.* **2019**, *21* (42), 23626-23637.

(62) Ma, Y.; Balbuena, P. B., Surface Segregation in Bimetallic Pt_3M (M=Fe, Co, Ni) Alloys with Adsorbed Oxygen. *Surf. Sci.* **2009**, *603* (2), 349-353.

(63) Hoshino, T.; Zeller, R.; Dederichs, P. H.; Weinert, M., Magnetic Energy Anomalies of 3d-Systems. *Europhys. Lett.* **1993**, *24* (6), 495-500.

(64) Menning, C. A.; Chen, J. G., Thermodynamics and Kinetics of Oxygen-Induced Segregation of 3d-metals in Pt–3d–Pt(111) and Pt–3d–Pt(100) Bimetallic Structures. *J. Chem. Phys.* **2008**, *128* (16), 164703.

(65) He, Y.; Wu, Y. L.; Zhu, X. X.; Wang, J. N., Remarkable Improvement of the Catalytic Performance of PtFe Nanoparticles by Structural Ordering and Doping. *ACS Appl. Mater. Inter.* **2019**, *11* (12), 11527-11536.

(66) Sáenz-Trevizo, A.; Hodge, A. M., Nanomaterials by Design: a Review of Nanoscale Metallic Multilayers. *Nanotechnology* **2020**, *31*, 292002.

(67) Svalov, A.V., Vas'kovskiy, V.O., Kurlyandskaya, G.V., Influence of the Size and Structural Factors on the Magnetism of Multilayer Films Based on 3d and 4f Metals. *Phys. Metals Metallogr.*, **2017**, *118*, 1263–1299.

(68) Kresse, G.; Hafner, J., Ab Initio Molecular Dynamics for Liquid Metals. *Phys. Rev. B* **1993**, *47* (1), 558-561.

(69) Kresse, G.; Hafner, J., Ab Initio Molecular-Dynamics Simulation of the Liquid-Metal--Amorphous-Semiconductor Transition in Germanium. *Phys. Rev. B* **1994**, *49* (20), 14251-14269.

(70) Kresse, G.; Furthmüller, J., Efficiency of Ab-Initio Total Energy Calculations for Metals and Semiconductors using a Plane-Wave Basis Set. *Comp. Mater. Sci.* **1996**, *6* (1), 15-50.

(71) Kresse, G.; Furthmüller, J., Efficient Iterative Schemes for Ab Initio Total-Energy Calculations using a Plane-Wave Basis Set. *Phys. Rev. B* **1996**, *54* (16), 11169-11186.

(72) Perdew, J. P.; Ruzsinszky, A.; Csonka, G. I.; Vydrov, O. A.; Scuseria, G. E.; Constantin, L. A.; Zhou, X.; Burke, K., Restoring the Density-Gradient Expansion for Exchange in Solids and Surfaces. *Phys. Rev. Lett.* **2008**, *100* (13), 136406.

(73) Dudarev, S. L.; Botton, G. A.; Savrasov, S. Y.; Humphreys, C. J.; Sutton, A. P., Electron-Energy-Loss Spectra and the Structural Stability of Nickel Oxide: An LSDA+U study. *Phys. Rev. B* **1998**, *57* (3), 1505-1509.

(74) Blöchl, P. E., Projector Augmented-Wave Method. *Phys. Rev. B* **1994**, *50* (24), 17953-17979.

(75) Kresse, G.; Joubert, D., From Ultrasoft Pseudopotentials to the Projector Augmented-Wave Method. *Phys. Rev. B* **1999**, *59* (3), 1758-1775.

(76) Monkhorst, H. J.; Pack, J. D., Special Points for Brillouin-Zone Integrations. *Phys. Rev. B* **1976**, *13* (12), 5188-5192.

For Table of Content Only